Journal of Power Sources 196 (2011) 8747–8754

Contents lists available at ScienceDirect

Journal of Power Sources

journal homepage: www.elsevier.com/locate/jpowsour

On the aggregate grid load imposed by battery health-conscious charging of plug-in hybrid electric vehicles

Saeid Bashash[a,*], Scott J. Moura[b], Hosam K. Fathy[a]

[a] Control Optimization Laboratory, Mechanical and Nuclear Engineering Department, The Pennsylvania State University, United States
[b] Automated Modeling Laboratory, Department of Mechanical Engineering, University of Michigan, Ann Arbor, United States

ARTICLE INFO

Article history:
Received 19 May 2011
Accepted 5 June 2011
Available online 12 June 2011

Keywords:
Plug-in hybrid electric vehicles
Grid load modeling
Lithium-ion battery degradation

ABSTRACT

This article examines the problem of estimating the aggregate load imposed on the power grid by the battery health-conscious charging of plug-in hybrid electric vehicles (PHEVs). The article begins by generating a set of representative daily trips using (i) the National Household Travel Survey (NHTS) and (ii) a Markov chain model of both federal and naturalistic drive cycles. A multi-objective optimizer then uses each of these trips, together with PHEV powertrain and battery degradation models, to optimize both PHEV daily energy cost and battery degradation. The optimizer achieves this by varying (i) the amounts of charge obtained from the grid by each PHEV, and (ii) the timing of this charging. The article finally computes aggregate PHEV power demand by accumulating the charge patterns optimized for individual PHEV trips. The results of this aggregation process show a peak PHEV load in the early morning (between 5.00 and 6.00 a.m.), with approximately half of all PHEVs charging simultaneously. The ability to charge at work introduces smaller additional peaks in the aggregate load pattern. The article concludes by exploring the sensitivity of these results to the relative weighting of the two optimization objectives (energy cost and battery health), battery size, and electricity price.

1. Introduction

This article examines the problem of estimating the total load imposed on the power grid by an aggregate set of plug-in hybrid electric vehicles (PHEVs).[1] Such PHEV load estimation can be particularly important for at least two reasons. First, an understanding of PHEV-induced grid load may be valuable for scheduling grid generation dispatch to accommodate this load [1]. Second, in the longer term, predicting PHEV power demand may be necessary in order for the electric utility infrastructure to expand accordingly.

The literature already provides several comprehensive studies examining the impact of vehicle electrification on overall grid load [2–4], the grid's ability to accommodate intermittent renewable energy [5,6], grid load control [1,7], and greenhouse gas emissions [8–10]. All these studies treat PHEVs as intermediaries between the transportation and power infrastructures, with the ability to store energy electrochemically when available for later use when needed for either propulsion or grid services such as load leveling, etc. The fact that the electrochemical batteries used for such storage are currently expensive, and degrade with usage, creates impetus for research on battery health degradation within the V2G framework [11].

Recent research by the authors explored the interplay between battery health and V2G integration by optimizing the daily charge pattern of a single PHEV to minimize both its energy consumption cost and battery degradation [12]. This research showed that the optimal charge pattern for a PHEV depends significantly on the interplay between trip length, trip timing, and electricity pricing. The research modeled battery health degradation using an electrochemistry-based model of lithium-ion batteries [13–15]. This model's parameters were optimized to fit both short-term experimental battery cycling data obtained by the authors as well as longer-term aging data from manufacturer tests [12]. The incorporation of a battery health degradation phenomenon (namely, solid electrolyte interphase, or SEI, layer growth) as a charge pattern optimization objective furnished *last-minute* charging patterns where PHEVs demanded grid electricity immediately prior to trip inception. This contrasted significantly with the more traditional *late afternoon* and *overnight* charging patterns examined in earlier literature.

This article extends the above research by optimizing the charge pattern for a fleet of PHEVs following a representative set of daily driving cycles. We use a mid-size power-split PHEV model to evaluate the energy costs associated with these drive cycles, and use the

* Corresponding author. Tel.: +1 864 650 7539; fax: +1 814 865 7222.
E-mail address: sub34@psu.edu (S. Bashash).

[1] A preliminary version of the results included in this article was presented at the 2010 ASME Dynamic Systems and Control Conference [28]. The authors gratefully acknowledge the copyright release granted by ASME for the material presented in that effort.

0378-7753/$ – see front matter © 2011 Elsevier B.V. All rights reserved.
doi:10.1016/j.jpowsour.2011.06.025

above mentioned electrochemistry-based battery model to examine PHEV battery degradation. The drive cycle start times, end times, and travel distances are generated based on travel data provided by the National Household Travel Survey (NHTS). Furthermore, the actual velocity-versus-time trajectory for each drive cycle is generated from a Markov chain model fitted to standard and naturalistic drive cycles. We obtain aggregate PHEV power demand by accumulating the individual optimal PHEV charge patterns for the above cycles. The results of this aggregation show that aggregate PHEV load peaks early in the morning, with nearly half of all PHEVs charging simultaneously. Moreover, the ability to charge at work can add further, smaller peaks to this aggregate load. The occurrence of such secondary peaks depends significantly on whether electricity price is flat throughout the day or varies between on-peak and off-peak hours.

The remainder of this article is organized as follows: Section 2 presents a method for generating a set of representative synthetic trips for PHEVs. Section 3 introduces the PHEV model and the lithium-ion battery model, and formulates the charge pattern optimization problem. Section 4 computes aggregate PHEV power demand, and Section 5 summarizes the article's main findings.

2. Synthetic trip generation

This section presents a set of representative synthetic trips, or drive cycles, for a population of PHEVs. We generate these trips using a three-step process: First, we re-sample a set of trip start times and trip lengths from the statistical distributions of these variables, which we obtain from the NHTS data repository. Second, we use a Markov chain model previously fitted to a set of both federal and real-world drive cycles to generate profiles of vehicle velocity versus time. Third, we combine the re-sampled NHTS data with the velocity profiles produced by the Markov chain to obtain a set of representative daily trips for PHEVs.

2.1. Travel data

NHTS provides a large pool of real-world driving data to assist transportation planners and policy makers in understanding travel patterns in the United States [16]. These data include the timing, the lengths, and the purposes of various daily trips taken by thousands of different drivers. NHTS groups the purposes of these trips into categories such as going to work, returning from work, family/personal business, school/church, etc. This work focuses on NHTS travel patterns consisting of only two work-related trips per day, i.e., going to and returning from work. One of the objectives of this effort is to examine the extent to which PHEVs benefit from additional charging at work, versus charging at home only.

From the 2001 NHTS records corresponding to nearly 150,000 different drivers, we choose the statistics of 8500 drivers who commuted between home and work using their personal vehicles (as compared to, say, rail transportation). Fig. 1 shows the histograms of the first and second trip start times and the trip lengths (i.e., travel distances), noting that the distribution of the first trip length (home to work) and second trip length (work to home) are nearly identical. The peak values of the departure times for the first and second trips are between 6:00 and 7:00 a.m., and between 5:00 and 6:00 p.m., respectively. Moreover, the peak value of the trip length distribution falls in the range of 5–10 miles.

Since the size of the selected data is too large for the PHEV charge pattern optimization study, we re-sample the NHTS data to generate a smaller set of representative trips from the distributions shown in Fig. 1. To perform this re-sampling, we begin by computing the statistical correlations between selected variables from the NHTS data, as shown in Table 1. The results show that the first

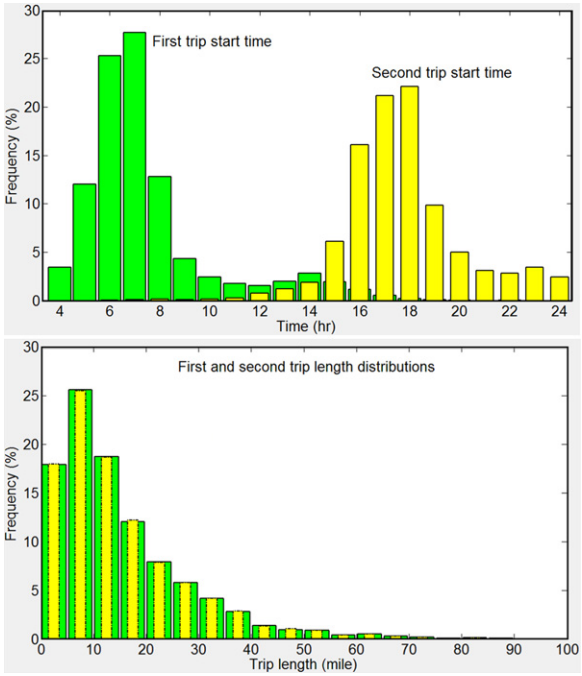

Fig. 1. Histograms of (a) trip start time, and (b) trip length for the two-way work trips obtained from about 8500 drivers data in the NHTS dataset [16].

and second trips are very strongly correlated in length (correlation coefficient of 0.99), which is consistent with this study's focus on two-part daily commutes from home to work and back. The results also show a strong correlation between the first and second trip start times (correlation coefficient of 0.68). Finally, the correlations between trip start times and trip lengths are relatively weak. Therefore, we re-sample the NHTS data in a manner that maximizes the correlation between trip start times, but minimizes the correlation between trip lengths and trip start times. The latter goal is accomplished using a minimum-correlation Latin hypercube selection procedure [17]. Table 2 presents the timing and lengths of 20 trips re-sampled from the NHTS distribution using this process, and used throughout the remainder of this article.

2.2. Velocity data

While Table 2 gives the overall characteristics of the re-sampled trips used in this study, it does not provide instantaneous profiles of vehicle velocity versus time for each of these trips. To generate a set of representative velocity profiles, we use a Markov chain model capturing vehicle drive cycle characteristics [18,19]. The Markov chain provides a statistical representation of the evolution of vehicle velocity versus time, in the form of a transition matrix relating acceleration at every time instant to previous velocities and accelerations. The transition probabilities of this Markov chain are identified from a set of vehicle certification cycles (FTP-72, US06, HWFET) and real-world micro-trips (WVUCITY, WVUSUB, WVUINTER) from the ADVISOR database [20] via maximum likelihood estimation. We simulate this Markov chain model for the different trip lengths in Table 2, thereby obtaining a velocity-versus-time profile for each trip.

Fig. 2 depicts a sample velocity profile generated for the first part of Trip #10 of Table 2, starting at 7:01 a.m. with the lengths of 28.49 miles. It is worthwhile to note that the Markov chain model generates velocity profiles stochastically, resulting in different trip durations for the same trip length. However, since the total energy consumption of a PHEV is tightly related to its trip length, the Markov chain model can be reasonably used for synthetic trip

Table 1
Correlation coefficients between the variables selected from the NHTS dataset.

	First trip start time	First trip length	Second trip start time	Second trip length
First trip start time	1.00	−0.17	0.68	−0.16
First trip length	−0.17	1.00	−0.01	0.99
Second trip start time	0.68	−0.01	1.00	−0.01
Second trip length	−0.16	0.99	−0.01	1.00

Table 2
Schedule and length of 20 re-sampled trips from the NHTS distributions.

Trip #	First trip start time	Second trip start time	Trips length (mile)	Trip #	First trip start time	Second trip start time	Trips length (mile)
1	4:35	12:07	11.47	11	7:14	17:00	14.53
2	5:17	14:13	10.00	12	7:27	17:03	15.80
3	5:36	14:57	7.83	13	7:32	17:15	18.36
4	5:57	15:14	24.36	14	7:47	17:22	3.09
5	6:08	15:19	1.26	15	8:01	18:00	5.03
6	6:24	15:49	9.02	16	8:24	18:18	53.28
7	6:30	16:01	6.00	17	9:03	19:10	34.94
8	6:40	16:15	6.90	18	10:33	20:31	12.50
9	6:55	16:18	20.76	19	13:18	22:10	2.17
10	7:01	16:40	28.49	20	15:36	24:31	4.29

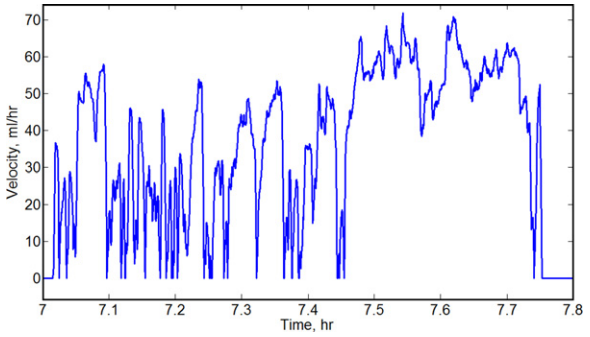

Fig. 2. A sample velocity profile generated for the first part of Trip #10 of Table 2, with trip length of 28.49 miles starting at 7:01 a.m.

development. Fig. 3 depicts all of the 20 representative drive cycles generated through the Markov chain model.

3. PHEV charge pattern optimization

This section examines the problem of optimizing the timing and amount of PHEV charging for each of the above 20 drive cycles. We perform this optimization using a previously developed multi-objective charge pattern optimizer described in more detail in Ref. [12]. The optimization objective is to simultaneously minimize (i) the total energy cost (fuel plus electricity) and (ii) the total battery degradation for each of the drive cycles. The first objective is calculated using a previously developed stochastic optimal PHEV power management strategy [19,21], whereas the second objective is evaluated through an electrochemistry-based model of anode-side resistive film formation in lithium-ion batteries [13,14]. Because these two objectives are conflicting, we trade them off using a non-dominated sorting genetic algorithm, NSGA-II [22]. This section briefly reviews the PHEV model, the battery model, and their use in the PHEV charge pattern optimization problem.

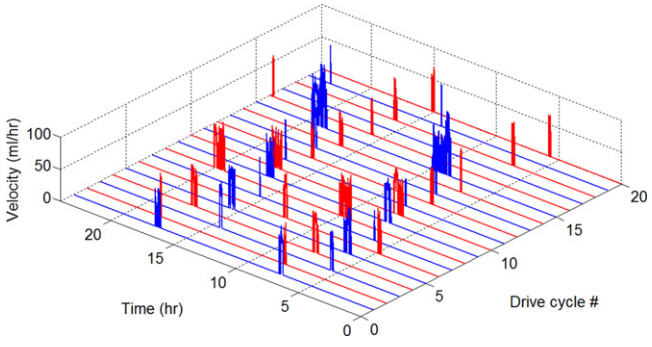

Fig. 3. Representative dive cycles generated using the NHTS data distributions and the Markov chain model.

3.1. PHEV model with optimal power management

The PHEV model used in this effort is based on a power-split mid-size sedan vehicle, similar in configuration, dynamics, and design to the 2002 Toyota Prius (see Fig. 4). The supervisory power management algorithm, which determines the optimal split of engine and battery power, is developed using stochastic dynamic programming (SDP) techniques. The details of the model and the optimal power management algorithm can be found in Ref. [19]. Here, we present a simulation study of the model to provide an insight into how battery state-of-charge (SOC) at the beginning of a trip can affect the PHEV fuel and overall energy consumption costs over the trip.

The results of this simulation are shown in Fig. 5, where the final values of energy consumption costs for the first part (home-to-work) of Trip #10 (shown in Fig. 2) are plotted against the initial battery SOC. Fuel and electricity prices are chosen based on the average rates of the year 2008 in the United States. From Fig. 5, we see that increasing the initial battery SOC increases trip electricity

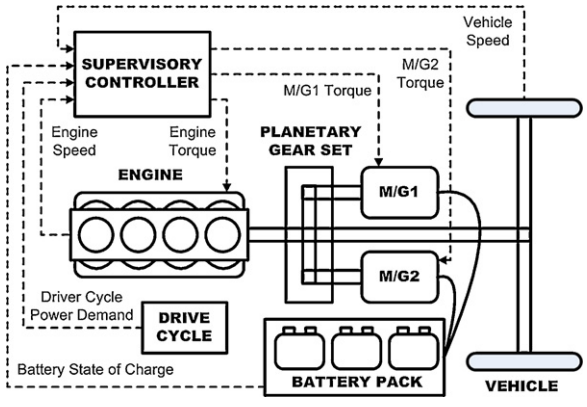

Fig. 4. PHEV model components, supervisory controller, and signal flow.

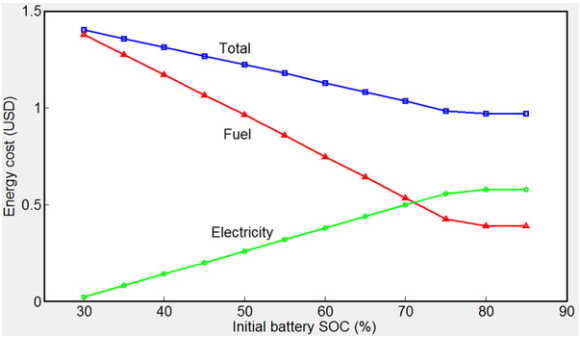

Fig. 5. Fuel, electricity, and total energy costs versus initial battery SOC for the first part of Trip #10.

cost, but decreases both trip fuel cost and total energy cost. These trends cease above 80% initial SOC because the trip does not require more battery electricity beyond that point. Thus, we observe that to minimize total energy cost for a given trip, one must add enough charge to the battery, prior to that trip, to meet the trip's electrical energy needs. Our next goal is to use a fundamental lithium-ion battery model to understand the impact of such a charging approach on battery degradation.

3.2. Lithium-ion battery model

This article adopts a first-principles lithium-ion battery model from the electrochemistry literature [13,14]. This model simulates solid electrolyte interphase (SEI) growth, and treats it as a key contributor to battery capacity fade during energy storage and cycling. The model uses a set of Butler–Volmer electrochemical reaction equations and lithium-ion diffusion sub-models to build a detailed representation of the dynamics of lithium-ion batteries. Degradation, in this model, is represented by a side intercalation reaction occurring in the negative battery electrode (anode), and causing the irreversible loss of lithium ions to a growing solid electrolyte interphase film.

Let J_{sd} represents the side reaction intercalation current density, and δ_{film} represents the resistive film thickness. Then the rate of increase of the resistive film is governed by a first-order differential equation given by:

$$\frac{\partial \delta_{\text{film}}(z,t)}{\partial t} = -k_1 J_{sd}(z,t) \tag{1}$$

where z represents the coordinate axis passing through the battery electrodes and separator, and k_1 is a constant coefficient containing a set battery parameters such as the molecular weight and density of the side reaction product. As the resistive film develops on the negative electrode, the battery SEI resistivity increases proportionally, as follows:

$$R_{SEI}(z,t) = R_{SEI}(z,t_0) + \frac{\delta_{\text{film}}(z,t)}{K_p} \tag{2}$$

where $R_{SEI}(z,t_0)$ denotes the initial SEI resistivity, and K_p represents the conductivity of the side reaction product.

The growth of the battery SEI resistivity provides a measure of battery health degradation for the multiobjective optimization problem examined in this effort. To quantify this resistivity increase, we simulate the full battery model and compute the side reaction intercalation current density, J_{sd}, while the battery is being charged, discharged, or kept steady in the storage mode. This article omits the full description of the battery model for brevity, but encourages interested readers to study Refs. [13,14] for the details of the model, and Ref. [15] for a reduced-order version of the model adopted in this article for computational efficacy.

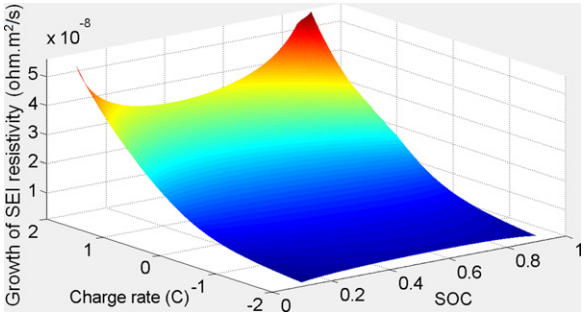

Fig. 6. Battery degradation map.

To illustrate the main features of the above degradation model, we present a static response surface map relating the rate of battery resistivity growth to battery SOC and charge/discharge rate (see Fig. 6). This map is obtained by simulating the battery model for an SOC range of 10–90% and charging rates of $-2C$ to $+2C$, with the negative sign indicating discharge. The parameters of the model are selected based on the results of an experimental system identification process on a set of lithium-ion battery cells with an $LiFePO_4$ cathode chemistry [A123], in a 26650 format [23]. The details of the experimental setup and the system identification process can be found in Ref. [12].

We can see from Fig. 6 that at the low and high SOC ends the battery tends to degrade faster, especially when it is subject to high-rate charging. Moreover, battery degradation takes place at a slower pace during charge depletion. To examine battery capacity fade during floating storage (i.e., when SOC is constant), we plot a sub-trajectory of the map corresponding to the charge rate of zero, as shown in Fig. 7. This sub-trajectory shows that the battery degradation rate is higher at higher SOC levels. Thus, storage at higher battery charge levels results in faster degradation. Similar trends have been obtained from the empirical analyses of different lithium-ion battery chemistries [24,25]. A key implication of this observation is that there is a non-trivial tradeoff between energy cost and battery health in the context of PHEV charging, since a higher battery SOC immediately prior to trip inception reduces trip energy cost but increases instantaneous battery degradation. Our next goal is to use multi-objective optimization to address this non-trivial tradeoff.

3.3. PHEV charge pattern optimization

In this section, we optimize the charge patterns of PHEVs for total energy cost and battery longevity. We adopt the optimization problem formulation developed in Ref. [12], where the optimization variables are the time at which each PHEV charging event begins, and the amount by which the PHEV's SOC changes over

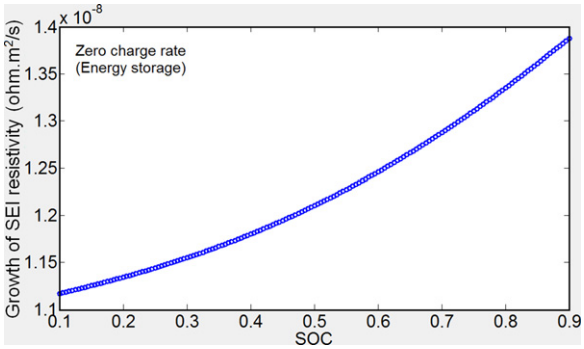

Fig. 7. Battery degradation trend in the energy storage mode.

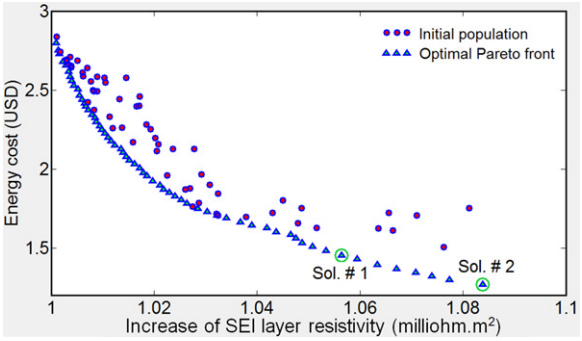

Fig. 8. Charge pattern optimization of the PHEV model with a 12 kWh battery for drive cycle #10.

the event. The number of charging events depends on whether the PHEVs are able to charge at home only (1 event per day), or home and work (2 events per day). The constant-current/constant-voltage (CCCV) charging strategy is adopted, and an SOC cap of 90% is imposed.

For a drive cycle with N separate trips the optimization objective is to:

$$\underset{x}{\text{Minimize}} \left\{ \left(f_1(x) = \int_{24\,\text{h}} J_{\text{fuel}}(x,t)dt + \int_{24\,\text{h}} J_{\text{elec}}(x,t)dt \right) \text{ and } \left(f_2(x) = \tilde{R}_{\text{film}}^{24\,\text{h}}(x) \right) \right\} \quad (3)$$

$x = [x_1, x_2, x_3, \ldots, x_{2N}]$

$x_{2i-1},\ i = 1, 2, \ldots, N\,(i.e.,\ x_1,\ x_3, \ldots x_{2N-1})$: Start time of charging for trip i

$x_{2i},\ i = 1, 2, \ldots, N\,(i.e.,\ x_2,\ x_4, \ldots x_{2N})$: Charge amount for rip i (up to 90% SOC)

where J_{fuel} and J_{elec} are the instantaneous fuel and electricity dollar costs per unit time, $\tilde{R}_{\text{film}}^{24\,\text{h}}$ is the final value of the anode-side resistivity growth at the end of the 24-h simulation, and x is the vector of optimization variables defining the charge patterns. We set the charging power of PHEVs to a constant rate of 2 kW, which corresponds to a typical residential charger. Finally, the lower and upper bounds of the variables associated with the charge times are set such that the entire dwell time between the trips can potentially be used for charging.

Two different electricity pricing policies are adopted for the optimization studies in the article. First, we use the DTE energy pricing policy for electric vehicles in the State of Michigan within the period of June to September 2009 [26]. This policy consists of two different rates: During the on-peak hours (10.00 a.m. until 7.00 p.m.) the electricity rate is 0.099 USD kWh^{-1}, while during the off-peak hours this rate reduces to 0.035 USD kWh^{-1}. Second, we examine a flat electricity price of 0.117 USD kWh^{-1}, corresponding to the average United States residential electricity price for the year 2009 [27].

To account for charging location, we consider two PHEV charging scenarios: (i) charging at home only, and (ii) charging at home and at work. Therefore for the first scenario, where there is only one charging event, the optimization problem consists of two variables, whereas in the second scenario the optimization problem includes four variables.

The method of NSGA-II [22] is used to carry out the multi-objective optimization tasks developed in this article. Fig. 8 depicts an example of the optimal solutions obtained for the PHEV model with a battery size of 12 kWh, following drive cycle #10, and adopting the second charging scenario (i.e., charging at home and at work). These solutions constitute a Pareto front: a set of charge patterns that represents the best attainable combinations of energy cost versus battery health. Ideally, no point on this Pareto front can be "dominated", meaning that there cannot exist a charge pattern that improves upon the Pareto front in terms of both energy cost and battery longevity. We obtained this Pareto front after running NSGA-II for 50 generations and 60 population members.

Fig. 9 shows charge patterns corresponding to two sample solutions from this Pareto front. Two main observations can be made from these charge patterns: First, both charging tasks take place during off-peak hours. Second, the charge pattern before the first trip immediately precedes the trip's onset. This keeps battery degradation caused by energy storage at high SOC relatively small since the PHEV discharges the battery immediately after charging it.

4. PHEV power demand computation

Section 3 of this article presented an approach for optimizing the PHEV charge pattern corresponding to a specific daily trip, such that PHEV energy cost and battery degradation are minimized. This section computes the aggregate demand for multiple PHEV trips (specifically, for the 20 trips from Section 2) by choosing and accumulating individual charge patterns from the individual Pareto fronts corresponding to each PHEV trip. This process involves selecting a single representative charge pattern from each Pareto front, which is carried out through a secondary optimization process described next.

4.1. Selection of charge patterns from the Pareto fronts

To select a representative charge pattern from a Pareto front, we normalize the objective functions with respect to their mean

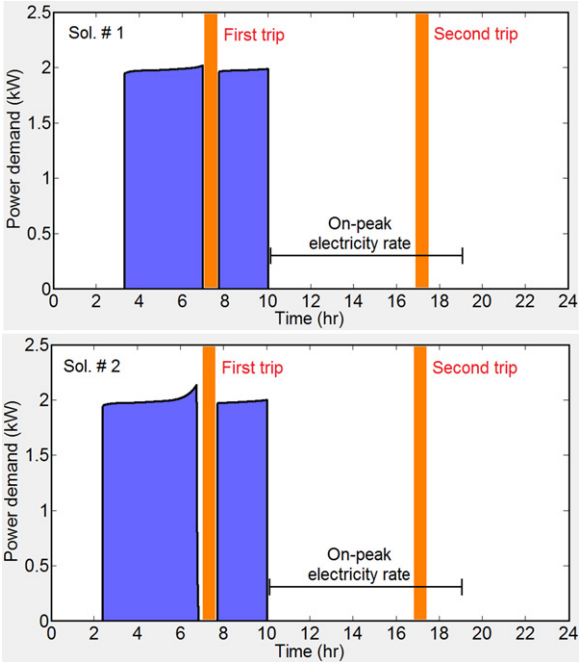

Fig. 9. Two sample charge patterns from the optimal Pareto front.

values in the Pareto front, and then minimize their weighted sum over the existing solutions in the Pareto front:

$$\underset{x\_\text{Pareto}}{\text{Minimize}}\, f = f_{1n} + \alpha f_{2n} \tag{4}$$

where f_{1n} and f_{2n} are the normalized battery degradation and energy cost objectives, respectively, and α is the weighting coefficient. The above optimization problem is a single-variable single-objective optimization problem over a finite set, which can be easily solved by choosing a value for α and evaluating the entire Pareto set for the above objective function. A large value of α puts more emphasis on the second objective (energy cost) compared to the first objective (battery degradation), and vice versa. For example, from the charge patterns shown in Fig. 8, Sol. #1 corresponds to α value of 0.1, whereas Sol. #2 corresponds to α value of 0.3 or higher. Most of the results presented in the following section use a value of 1 for α, thereby placing equal emphasis on the two optimization objectives. However, we also examine the case of using different values of α, to show how the tradeoff between the two optimization objectives can affect the aggregate PHEV load pattern.

4.2. Aggregate PHEV load patterns

We obtain the aggregate PHEV load pattern by choosing a battery size, a charging scenario (i.e., charging at home versus both work and home), an electricity pricing policy, and a value for the weighting coefficient α, and then optimizing and accumulating the individual charge patterns for all the 20 trips studied in this article. Therefore, different load patterns can be generated for different selections of the above parameters. In this section, we first discuss the PHEV load pattern obtained for a nominal selection of the above parameters, and then we examine the effect of varying each parameter relative to its nominal value.

Fig. 10 depicts the battery health-conscious aggregate load pattern for a population of PHEVs with 12 kWh batteries, allowed to charge both at home and at work, with on/off-peak electricity pricing, for a unity value of the weighting parameter α. The most salient features of this load pattern can be summarized as follows:

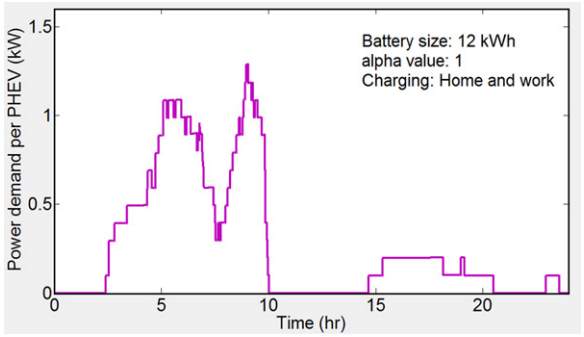

Fig. 10. Aggregate power demand for PHEVs with 12 kWh battery for $\alpha = 1$, home and work charging, and stepped on-peak/off-peak electricity pricing.

- The first PHEV peak load occurs between 5:00 and 6:00 a.m. with about 50% of the PHEVs simultaneously receiving electricity from the grid (note that this peak load corresponds to approximately 1 kW per PHEV, while the charging rate of each PHEV is 2 kW).
- There is a secondary peak around 9:00 a.m. with about 60% of PHEVs connected to the grid. This peak represents a "rush" by PHEVs to charge their batteries during off-peak hours, immediately after arriving at work.
- There is sudden drop in the load pattern at 10:00 a.m., which corresponds to the rise of electricity price to the on-peak rate.
- Except for the time period from 2:00 a.m. to 10:00 a.m., the number of PHEVs charging from grid remains below 10% of the total PHEV population.

These observations correspond to the specific choices of optimization parameters listed at the beginning of this section. Next, we vary these optimization parameters individually and examine the effect of such variation on the aggregate PHEV load pattern.

4.2.1. Effects of optimization tradeoff

Fig. 11 shows the aggregate PHEV load patterns for four different values of the objective weighting parameter, $\alpha = 0.01$, 0.1, 10, and

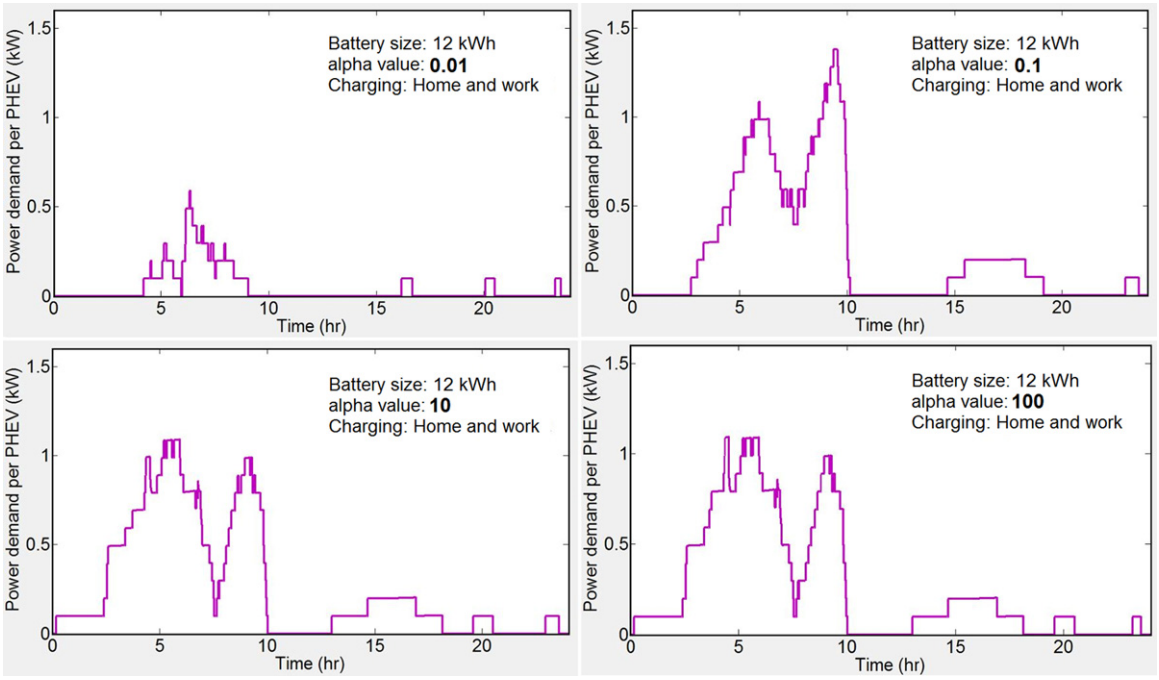

Fig. 11. The effects of the weighting parameter, α, on the aggregate PHEV power demand (12 kWh battery, home and work charging, and stepped on-peak/off-peak electricity pricing).

Table 3
Average electricity demand, average energy cost, and average battery SEI resistivity growth for PHEVs with different parameter sets.

Parameter set	Avg. electric energy per PHEV (kWh)	Avg. energy cost per PHEV (USD)	Avg. SEI res. growth ($m\Omega\,m^2$)
12 kWh, $\alpha = 1$, H W^{-1} (on/off-peak pricing)	6.38	0.78	1.03
12 kWh, $\alpha = 0.01$, H W^{-1} (on/off-peak pricing)	1.10	1.37	1.00
12 kWh, $\alpha = 0.1$, H W^{-1} (on/off-peak pricing)	5.90	0.83	1.02
12 kWh, $\alpha = 10$, H W^{-1} (on/off-peak pricing)	6.38	0.78	1.03
12 kWh, $\alpha = 100$, H W^{-1} (on/off-peak pricing)	6.38	0.78	1.03
8 kWh, $\alpha = 1$, H W^{-1} (on/off-peak pricing)	5.85	0.83	1.04
16 kWh, $\alpha = 1$, H W^{-1} (on/off-peak pricing)	6.46	0.78	1.02
12 kWh, $\alpha = 1$, H only (on/off-peak pricing)	5.17	0.88	1.03
12 kWh, $\alpha = 1$, H W^{-1} (flat pricing)	6.15	1.27	1.01

100 (note that case of $\alpha = 1$ has already been examined). Increasing the value of α favors the energy cost objective. This causes PHEVs to demand more grid electricity, since it is cheaper for propulsion than fuel. The overall effect is an increase in aggregate electricity demand together with a drop in total PHEV energy cost and a slight increase in battery health degradation. For example, Increasing α from 0.01 to 0.1 causes PHEVs to demand 436% more electricity from the grid, reduces their total daily energy cost by 39%, and increases their overall battery degradation by approximately 2% (see Table 3). Increasing α further from 0.1 to 1 increases total electricity demand by 18% more, reduces total energy cost by 6% more, while increasing battery degradation by approximately 1% more. There is almost no change in the load profile if we increase α further.

4.2.2. Effects of battery size

Fig. 12 shows the aggregate PHEV load patterns for 8 kWh and 16 kWh batteries. The rest of the parameters are kept the same as the initial/nominal values. We see that the shape of the overall PHEV load pattern does not change qualitatively with battery size. The main quantitative consequence of doubling battery size from 8 kWh to 16 kWh is a 6% reduction in consumer energy cost, and a simultaneous 2% improvement in battery health (see Table 3). These improvements can be explained as follows: larger batteries make it possible to drive further on electricity (which is cheaper), with less of a need to push the batteries to high SOC values (which can cause induce more degradation). The benefits associated with larger batteries are more pronounced if PHEVs are unable to charge at work (i.e., if they charge at home only). In that case, increasing battery size from 8 kWh to 16 kWh corresponds to a 22% reduction in total energy cost.

4.2.3. Effect of charging location

Fig. 13(a) depicts the aggregate PHEV load pattern for the initial parameter set when only charging at home is available, as opposed to charging at both home and work. There is a single peak load in the morning (around 5 a.m.) with about 55% of PHEVs charging from the grid. The power demand drops at 10 a.m. but with a much smoother transition compared to the case where charging at work is also available. The ability to charge at work essentially allows PHEVs to obtain more electricity from the grid over the course of the day. This reduces the average consumer energy cost by 19% for 8 kWh batteries, and 1% for 16 kWh batteries. Further examination of Table 3 shows that the ability to charge at work does not affect battery degradation significantly. This is a consequence of two competing effects. On the one hand, charging at work allows PHEVs to reduce the charge added to their batteries before the first trip, thereby reducing battery degradation caused by energy storage between trips. On the other hand, PHEVs charge more on average when allowed to charge at both work and home, which

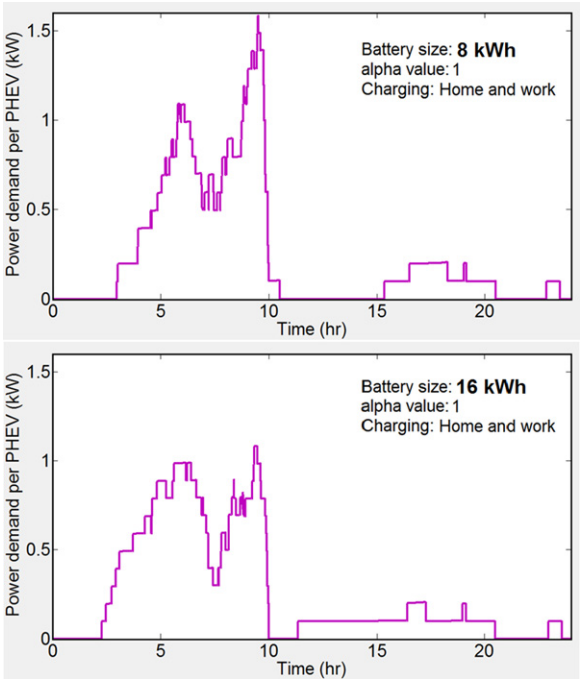

Fig. 12. The effects of battery size on the aggregate PHEV power demand ($\alpha = 1$, home and work charging, and stepped on-peak/off-peak electricity pricing).

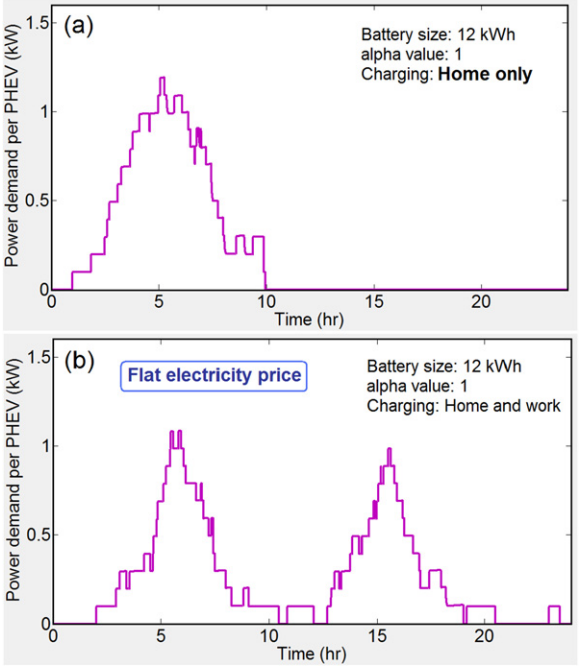

Fig. 13. Aggregate PHEV power demand for (a) home charging only and (b) home and work charging with flat electricity pricing (12 kWh battery, and $\alpha = 1$).

amplifies the degradation because of higher battery usage. These two effects largely nullify each other, resulting in the small impact of charging location on battery degradation.

4.2.4. Effects of electricity pricing

The presence of a large jump in the electricity price during the off-peak to on-peak transition moment creates load congestion before the transition time. To understand how much this jump affects the results shown so far, we compute the optimal charge patterns for the *flat* electricity pricing policy described in Section 3.3. Fig. 13(b) shows the corresponding aggregate load profile for the initial parameter set, i.e., 12 kWh battery, home and work charging, and $\alpha = 1$. Flat electricity pricing results in two nearly identical load patterns, one taking place in the morning and one in the afternoon. Gone are some of the salient features of Fig. 10 introduced by the onset of on-peak pricing, such as the secondary aggregate load peak shortly before 10:00 a.m. The sheer degree to which electricity pricing can change the shape of the optimal PHEV charge patterns underscores the viability of pricing as a tool for shaping aggregate PHEV power demand.

5. Summary and conclusions

This article examined the problem of predicting the aggregate grid load imposed by the battery health-conscious charging of plug-in hybrid electric vehicles (PHEVs). The article adopted a representative PHEV powertrain model developed previously by the authors to compute the on-road PHEV energy consumption costs. The article then used an electrochemistry-based lithium-ion battery model to predict the PHEV's battery health degradation over the course of a full daily drive cycle. Twenty representative sets of daily trip start times and trip lengths were re-sampled from the statistics of the NHTS database. For each of these sample trips, on-road vehicle velocity was generated as a function of time using a Markov chain model trained on both federal and naturalistic driving data. For each of the resulting daily trip descriptions, we used NSGA-II to obtain a Pareto set of PHEV charge patterns optimizing both total PHEV energy cost and battery health. Aggregating the resulting PHEV charge patterns furnished a prediction of the battery health-conscious PHEV grid load.

Unlike the PHEV-induced grid loads traditionally studied in the literature, our results show a peak load early in the morning (between 5.00 a.m. and 6.00 a.m.), immediately preceding departure to work. Moreover, if charging at work is provided, there are additional peaks immediately preceding the onset of on-peak electricity pricing, and possibly in the afternoon. During the peak load at 2 kW charge rate, approximately 50–60% of the PHEV population simultaneously receives electricity from the grid. The results obtained in this article are based on a particular PHEV configuration, a set of specific trips (i.e., work-related trips), a specific model of battery health degradation, and finally, the assumption that consumers will adopt the developed battery health-conscious charging policies. However, the methods proposed herein can be used to analyze PHEV grid loads under other optimization scenarios as well. Key factors for consideration in future PHEV grid load studies include real-time load management and full vehicle-to-grid (V2G) integration with bidirectional power flow.

Acknowledgment

This research was initially supported by a research partnership led by the University of Michigan and DTE Energy, and funded by a Michigan Public Service Commission Grant. Further support has been provided by the Pennsylvania State University's College of Engineering through the third author's startup grant. The authors gratefully acknowledge this support.

References

[1] I. Hiskens, D. Callaway, Proceedings of the IEEE, 99, 2011, pp. 184–199.
[2] D. Wu, D. Aliprantis, Presentation for NETSCORE 21, February, 2009.
[3] S. Hadley, A. Tsvetkova, Potential impacts of plug-in hybrid electric vehicles on regional power generation, ORNL/TM report, January 2008.
[4] W. Kempton, J. Tomic, Journal of Power Sources 144 (2005) 268–279.
[5] W. Kempton, J. Tomic, Journal of Power Sources 144 (2005) 280–294.
[6] V. Marano, G. Rizzoni, Proceedings of the IEEE International Conference on Vehicular Electronics and Safety, Columbus, OH, 2008.
[7] M. Takagi, K. Yamaji, H. Yamamoto, Vehicle Power and Propulsion Conference (VPPC), Dearborn MI, September, 2009, pp. 822–826.
[8] C.H. Stephan, J. Sullivan, Environmental Science and Technology 42 (2008) 1185–1190.
[9] R. Sioshansi, P. Denholm, Environmental Science and Technology 43 (2009) 1199–1204.
[10] H.G. Grimes-Casey, G.A. Keoleian, B. Wilcox, Environmental Science and Technology 43 (2009) 585–590.
[11] S.B. Peterson, J. Apt, J.F. Whitacre, Journal of Power Sources 195 (2010) 2385–2392.
[12] S Bashash, S.J. Moura, J.C. Forman, H.K. Fathy, Journal of Power Sources 196 (2011) 541–549.
[13] P. Ramadass, B. Haran, P. Gomadam, R. White, B. Popov, Journal of Electrochemical Society 151 (2004) A196–A203.
[14] S. Santhanagopalan, Q. Guo, P. Ramadass, R. White, Journal of Power Sources 156 (2006) 620–628.
[15] J. Forman, S. Bashash, H.K. Fathy, J.L. Stein, Journal of Electrochemical Society (2011).
[16] U.S. DOT, National Household Travel Survey (http://nhts.ornl.gov/).
[17] A. Owen, Journal of American Statistical Association 89 (1994) 1517–1522.
[18] T.W. Anderson, L.A. Goodman, Annals of Mathematical Statistics 28 (1957) 89–110.
[19] S.J. Moura, H.K. Fathy, D.S. Callaway, J.L. Stein, IEEE Transactions on Control Systems Technology 99 (2010) 1–11.
[20] W.B. Wipke, M.R. Cuddy, S.D. Burch, IEEE Transactions on Vehicular Technology 48 (1999) 1751–1761.
[21] S.J. Moura, D.S. Callaway, H.K. Fathy, J.L. Stein, Journal of Power Sources 195 (2010) 2979–2988.
[22] K. Deb, A. Pratap, S. Agarwal, T. Meyarivan, IEEE Transactions on Evolutionary Computation 40 (2002) 181–197.
[23] A123 Systems website: www.a123systems.com.
[24] A123 Systems, Development of battery packs for space applications, NASA Aerospace Battery Workshop, Huntsville, AL, 2007.
[25] M. Ichimura, M. Shimomura, K. Takeno, R. Shirota, J. Yakami, Proceedings of the 27th International Conference on Telecommunications, 2005, pp. 245–250.
[26] DTE Energy website, Residential Electric Rates: (http://www.dteenergy.com/residentialCustomers/billingPayment/rates/electric/resRates.html).
[27] US Energy Information Administration (EIA) Independent Statistics and Analysis: (http://www.eia.doe.gov/electricity/epm/table5_6_a.html).
[28] S. Bashash, S.J. Moura, H.K. Fathy, Proceedings of the 2010 ASME Dynamic Systems and Control Conference, Cambridge, MA, September, 2010.